Orbit Determination of Near Earth Asteroid 2003 HA22 using the Method of Gauss and Monte Carlo Simulations

ONL 7: Sunny Wang, Amanda Cao, Sarah Bewley

***Abstract*—Near Earth Asteroids (NEAs) pose a potentially devastating threat to Earth in the event of a collision, giving great importance to monitoring their orbits. This study aims to track the orbital path of the NEA 2003 HA22 using three separate observations of the asteroid, which were taken at the Cerro Tololo Observatory in La Serena, Chile and the NIRo Observatory in Indiana, USA across the month of July 2021. Once the images were obtained, the data was reduced and aligned, and the uncertainty was determined through Least Squares Plate Reduction in AstroImageJ with reference stars from the UCAC4 catalog in SAO DS9. In order to calculate the orbital elements, the Method of Gauss was used, using iteration to calculate increasingly accurate position vectors for a body. Using 10,000 Monte Carlo Simulations with the Method of Gauss, we obtain the following six orbital elements: a = 1.80064 AU, e = 0.372564, i = 1.54393 degrees, omega = 163.423 degrees, Omega = 122.032 degrees, and M = 365.675 degrees. The data was submitted to the Minor Planet Center to be used for tracking future encounters.**

***Index Terms*—Orbit Determination, Near-Earth Asteroid, Method of Gauss, Monte Carlo.**

I. Introduction

In addition to the commonly known planets, our solar system also boasts many forms of space debris. Some of the most frequently-occurring objects include comets and asteroids. Although the two terms are often confused, they refer to two distinct objects. Comets are composed of frozen chunks of rock, gas, and dust, and are recognized by their defining "trails", which occur when they heat up upon approaching the Sun [3]. Comets orbiting our Sun are largely found in the Kuiper Belt, which begins at around Neptune's orbit and extends to almost 1,000 AU from the Sun [10]. On the other hand, asteroids are defined as rocky objects that orbit the Sun; thus, they are also known as minor planets [1]. Asteroids are most commonly found within the asteroid belt, which spans between the orbits of Mars and Jupiter, however, they may occasionally stray closer to the Sun [2].

This study will be focused on Near Earth Asteroids (NEAs), which are defined as asteroids with orbits that are close to or crossing Earth's orbit [7]. Similarly, Mars-crossing asteroids are those that intersect Mars' orbit [6]. Although relatively unlikely, some NEAs may pose a threat to Earth in that there is a non-negligible risk of collision [9]. Thus, although there are no asteroids projected to strike the Earth within the next few hundred years, search campaigns are still crucial. Current search campaigns include NASA's Near Earth Object (NEO) Observation Program; as expected, this campaign combs the skies for potentially hazardous NEOs and NEAs. The NEO Observation Program especially focuses on objects larger than 1 kilometer, as these pose the greatest threat upon impact. Additionally, in 2014, a NEO Impact Working Group was approved; this group focuses on preparing disaster response measures for post-collision scenarios [5].

The NEA utilized in this report is 2003 HA22. To determine the orbit of an asteroid, six orbital elements are used. The following definitions of these elements are referenced from the Summer Science Program's OD 2021 Booklet. The first two orbital elements, the semi-major axis and the eccentricity, are concerned with the elliptical orbit of the asteroid. The semi-major axis refers to the longest diameter of the asteroid's elliptical orbit, and is used to measure the orbit's size. The eccentricity refers to the "shape" of the ellipse, where a lower eccentricity refers to a more circular orbit while a higher eccentricity corresponds with a more elongated orbit. The next three orbital elements are concerned with the relationship between the plane of the asteroid's orbit and the plane of Earth's orbit (the ecliptic). Firstly, inclination is the angle between the two planes, and is measured in degrees. Next, the longitude of the

ascending node is the angle between the Vernal Equinox (0 RA, 0 Dec) and the ascending node. The ascending node is the point at which the two planes intersect, where the asteroid begins moving from South to North in the ecliptic plane. Next is the argument of perihelion, which is the angle between the Vernal Equinox and the asteroid's closest point of passage to the Sun. The last orbital element is the mean anomaly, which is time dependent and is defined as the position of the asteroid if its orbit were circular, and is measured from the point of perihelion. Both this and the time of last perihelion passage may be used.

For the orbit determination process, we will be using the Method of Gauss, the steps of which will be outlined later in the report. The Method of Gauss is used in place of the Method of Laplace because the range to our asteroid is relatively small. In order for the Method of Gauss to be used, three observations of the asteroid must be taken. The time between these three observations should be roughly even.

II. Observations and image processing

A. Data Acquisition

During the course of SSP, our team submitted two observing requests that were successful and obtained images that were then processed. Both of these successful observing requests were located at Cerro Tololo Inter-American Observatory in Vicuña, Coquimbo, Chile. Our observations used the Prompt-6 telescope, which is an Optical and Polarimetry Telescope with a diameter of .04 meters. The PROMPT telescopes primarily use Alta U47+ cameras and E2V CCDs [8]. Images of asteroid 2003 HA22 were also taken at a group observation event for which our team was not responsible for submitting an observing request. Those images were taken at NIRo Observatory at Purdue University Northwest in Lowell, Indiana, United States, with an RCOS 20" telescope. The telescope has a diameter of 0.508 meters and a FLI PLO 9000 camera. The locations at which our observations were taken are displayed in Table I.

B. Image Reduction

Once we obtained our images, we started the process of image reduction. Using AIJ, we reduced, aligned, and stacked the images to get rid of high background noise and vignetting. Next, we took our 3 sets of 3 images created in the process and blinked them to determine the location of the asteroid. We then plate-solved the images in AIJ using Astrometry.net and determined the right ascension and declination of our asteroid. With plate-solved images we were able to select reference stars in DS9 using the UCAC4 catalog to determine the magnitude of our asteroid.

C. Determination of Errors in Astrometry

One method we used to determine errors in our astrometry was LSPR, or Least Squares Plate Reduction. A LSPR determines the RA and Dec of an object, as well as uncertainties in these values, using the centroids, RAs, and DECs of a set of reference stars. The LSPR reports for our 07/08 observation of 2003 HA22 at NIRo is shown in Table II.

We also calculated uncertainties using RMS (root mean squares) on corr.fits files obtained from plate solving using Astrometry.net. These uncertainties show us how our measured RA and Dec values differed from the expected values, using the following formulas:

$$\sqrt{\frac{1}{n}\sum_{j}(\alpha_j - \alpha_{0j})^2}$$

$$\sqrt{\frac{1}{n}\sum_{j}(\delta_j - \delta_{0j})^2},$$

where α and α_0 are the measured and expected RA values, and δ and δ_0 are the measured and expected DEC values.

D. Results

The results of our two observations of three images each, along with their uncertainties, are displayed in Table III.

Date/Time	Observatory	Images	Quality of Images
06/26 22:49 to 06:02 UTC	Fan Mountain Observatory, Virginia (RRRT)	N/A	N/A
06/29 01:52 to 04:20 UTC	Fan Mountain Observatory, Virginia (RRRT)	N/A	N/A
07/08 00:00 to 03:47 UTC	Cerro Tololo Observatory, La Serena	9	Good
07/14 01:37 to 05:24 UTC	Cerro Tololo Observatory, La Serena	9	Good
07/19 01:40 to 05:27 UTC	Cerro Tololo Observatory, La Serena	N/A	N/A

TABLE I
OBSERVATORIES USED.

Image Set	b1	b2	a11	a12	a21	a22	RA	DEC
1	236.70895	-15.11867	-0.0002911	-9.41546	3.8320984	0.0002823	15.76397	-14.9135
2	236.70895	-15.11867	-0.0002911	-9.41546	3.8320984	0.0002823	15.76397	-14.9135
3	236.70895	-15.11867	-0.0002911	-9.41546	3.8320984	0.0002823	15.76397	-14.9135

TABLE II
LSPR RESULTS.

Julian Date	RA	DEC	AbsMag	BoloMag	Diameter (km)	RA Uncert.	DEC Uncert.
2459403.515	15:58:49.70	-16:15:08.4	19.557	17.332	0.4208	5.85702e-05	2.1089e-05
2459403.532	15:58:52.89	-16:15:29.6	19.724	17.499	0.3896	5.80864e-05	2.4823e-05
2459403.547	15:58:55.69	-16:15:48.1	19.606	17.381	0.4114	1.31565e-04	4.8144e-05
2459409.601	16:21:50.21	-18:21:52.5	19.6269	17.4016	0.4075	9.94231e-05	9.6816e-05
2459409.602	16:22:00.15	-18:23:01	19.91	17.685	0.3577	9.40786e-05	6.5348e-05
2459409.603	16:21:50.63	-18:21:54.7	19.854	17.629	0.367	9.18694e-05	6.3729e-05

TABLE III
OBSERVATIONAL RESULTS.

III. ORBIT DETERMINATION

A. The Method of Gauss

Orbit determination was performed using the Method of Gauss, which is an iterative method for predicting the location of the asteroid using three evenly spaced out intervals, where the first and third observations are used in order to compute the second.

The fundamental triangle shown below relates the three vectors $\vec{r}$, $\vec{\rho}$, and $\vec{R}$, which represent the vectors from the Sun to the asteroid, Earth to the asteroid, and Sun to the Earth, respectively. Thus, we aim to find $\vec{r_2}$ and $\dot{\vec{r_2}}$, which are the position and velocity vectors of the asteroid for the middle observation.

The relationship between these vectors are given by

$$\vec{r} = \vec{\rho} - \vec{R}.$$

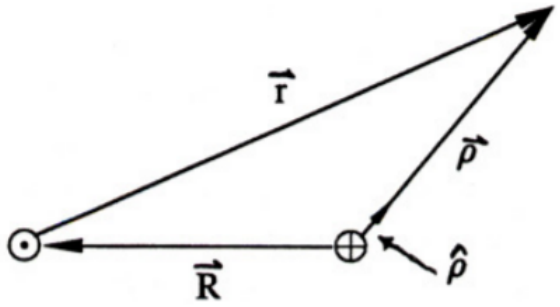

Fig. 1. The Fundamental Triangle. Adapted from the Orbit Determination Packet (2021).

From each observation, using the RA and DEC values, we can obtain $\hat{\rho}$, the unit vector pointing in the direction of the asteroid. MoG allows us to use $\hat{\rho}$ and the sun vector $\vec{R}$ to compute the position and velocity vectors $\vec{r_2}$ and $\dot{\vec{r_2}}$ through iteration.

A brief overview of the Method of Gauss is as follows:

1) Obtain an initial guess for $\vec{r_2}$ using the Scalar Equation of Lagrange.
2) Compute initial f and g expressions using a truncated second order Taylor series.
3) Compute the position vectors $\vec{r_1}$, $\vec{r_2}$, and $\vec{r_3}$.
4) Use the f and g expressions to compute an initial $\dot{\vec{r_2}}$.
5) Correct the time for the speed of light.
6) Iterate by recomputing f and g, using those to recompute the ρ values until the difference between subsequent rhos is less than a threshold, which we define as $1 \cdot 10^{-12}$.

The Method of Gauss was implemented in Python 3.9 using NumPy. Each step is discussed in further detail below.

1) Obtaining an initial $\vec{r_2}$: We begin by generating an estimate for $\vec{r_2}$ using the Scalar Equation of Lagrange. The equation is given by

$$r_2^8 + ar_2^6 + br_2^3 + c = 0.$$

Solving this eighth degree polynomial yields roots that serve as the initial guess for $\vec{r_2}$. Imaginary and negative roots are discarded. a, b, and c are derived from the times, the sun vectors, and $\hat{\rho}$.

2) Computing Initial f and g Values: The initial f and g values can be computed using a truncated second order Taylor series. These equations approximate f and g without the use of $\dot{\vec{r_2}}$, which we do not have yet:

$$f_i = 1 - \frac{\mu}{2r_2^3}\tau_i^2$$

$$g_i = \tau_i - \frac{\mu}{6r_2^3}\tau_i^3.$$

τ is the time (in Gaussian days) of the observation, r_2 is known from the Scalar Equation of Lagrange, and μ is 1 as we are working in Gaussian time.

3) Computing the Position Vectors $\vec{r_1}$, $\vec{r_2}$, $\vec{r_3}$: Using the f and g values, we can now compute the r values. First, using the known $\hat{\rho}$ vectors and the $\vec{R}$ vectors, we can compute ρ, also known as the scalar equations of range:

$$\rho_1 = \frac{c_1 \cdot D_{11} + c_2 \cdot D_{12} + c_3 \cdot D_{13}}{c_1 \cdot D_0}$$

$$\rho_2 = \frac{c_1 \cdot D_{21} + c_2 \cdot D_{22} + c_3 \cdot D_{23}}{c_2 \cdot D_0}$$

$$\rho_3 = \frac{c_1 \cdot D_{31} + c_2 \cdot D_{32} + c_3 \cdot D_{33}}{c_3 \cdot D_0},$$

where

$$c_1 = \frac{g_3}{(f_1 g_3 - g_1 f_3)}$$

$$c_3 = \frac{-g1}{f_1 g_3 - g_1 f_3}$$

$$c_2 = -1,$$

and

$$D_0 = \hat{\rho_1} \cdot (\hat{\rho_2} \times \hat{\rho_3})$$

$$D_{1j} = (\vec{R_j} \times \hat{\rho_2}) \cdot \hat{\rho_3}$$

$$D_{2j} = (\hat{\rho_1} \times \vec{R_j}) \cdot \hat{\rho_3}$$

$$D_{3j} = \hat{\rho_1} \cdot (\hat{\rho_2} \times \vec{R_j})$$

$$j = 1, 2, 3.$$

Then, we can use ρ to compute the position vectors.

$$\vec{r_1} = \hat{\rho_1} \cdot \rho_1 - R_1$$

$$\vec{r_2} = \hat{\rho_2} \cdot \rho_2 - R_2$$

$$\vec{r_3} = \hat{\rho_3} \cdot \rho_3 - R_3$$

This equation gives us an updated version of $\vec{r_2}$, as well as $\vec{r_1}$ and $\vec{r_3}$, which are needed to compute the velocity vector.

4) Computing the Velocity Vector $\dot{\vec{r_2}}$: The initial $\dot{\vec{r_2}}$ value can be computed using the equation

$$\dot{\vec{r_2}} = \frac{-f_3}{f_1 g_3 - f_3 g_1}\vec{r_1} + \frac{f_1}{f_1 g_3 - f_3 g_1}\vec{r_3}.$$

5) Light-travel Time Correction: Since the time that it takes for light to travel from the asteroid to the earth is non-negligible, we must account for this time. This can be done through the following equation:

$$t_i = t_{o,i} - \frac{\rho_i}{c}.$$

6) Iteration: Now, since we have all the initial values, we can iterate, recomputing f and g with $\vec{r_2}$ and $\dot{\vec{r_2}}$ and using them to calculate updated $\vec{r_2}$ and $\dot{\vec{r_2}}$ vectors. However, we can use the closed forms of f and g rather than the series, as it allows for more accurate computations. These equations are given below:

$$f_i = 1 - \frac{a}{r_2}[1 - \cos \Delta E_i]$$

$$g_i = \tau_i + \frac{1}{n}[\sin \Delta E_i - \Delta E_i].$$

To compute ΔE_i, we use the Newton-Raphson method with a tolerance of $1 \cdot 10^{-12}$ to numerically solve the equation

$$E - (1 - \frac{r_2}{a}) \sin E + \frac{\vec{r_2} \cdot \dot{\vec{r_2}}}{n \cdot a^2}(1 - \cos E) - n\tau_i.$$

Then, we use our new f and g to recompute $\vec{r_2}$ and $\dot{\vec{r_2}}$, iterating until the difference between subsequent rhos is less than $1 \cdot 10^{-12}$.

B. Limitations of the Method of Gauss

Due to its iterative nature, the Method of Gauss can potentially fail to converge. This is often a result of the three observations being too close to each other or lacking curvature. For this reason, we had to try several different combinations of three observations until one returned a successful result.

The successful set of three points consisted of two observations from observing group ONL 8 and one of our observations. The observations are displayed in Table IV.

Date	RA	DEC
2021 07 03 00:15:53	15:43:03.01	-14:37:19.2
2021 07 08 00:22:04	15:58:49.70	-16:15:08.4
2021 07 15 00:09:07	16:25:38.47	-18:40:50.7

TABLE IV
OBSERVATION INFORMATION USED FOR ORBIT DETERMINATION.

C. Monte Carlo Simulations

To simulate uncertainty in our orbit determination process, we used Monte Carlo simulations, which rely on sampling RA and DEC values from a normal distribution using the computed uncertainties. To implement this simulation, we used Python to randomly generate hundreds or even thousands of data points of our orbital elements. From these data points we were able to calculate a mean and a standard deviation, and create distribution plots showing these values as well as how they compared to values generated by JPL Horizons, an ephemera-generating database and interface created by the Jet Propulsion Laboratory [4].

D. Computing the Orbital Elements

The orbital elements can all be easily determined with $\vec{r_2}$, $\dot{\vec{r_2}}$, and the angular momentum $\vec{h}$, which is equivalent to $\vec{r_2} \times \dot{\vec{r_2}}$. The equations are given below. Some require a quadrant check, so two equations (the sin and cos) for the element are presented.

$$a = \frac{1}{\frac{2}{r} - v^2}$$

$$e = \sqrt{1 - \frac{h^2}{a}}$$

$$i = \tan^{-1} \frac{\sqrt{h_x^2 + h_y^2}}{h_z}$$

$$\begin{cases} \cos \Omega = -\frac{h_y}{h \sin i} \\ \sin \Omega = \frac{h_x}{h \sin i} \end{cases}$$

The argument of perihelion ω is given by

$$\omega = U - \nu$$

where

$$\begin{cases} \cos U = \frac{r_x \cos \Omega + r_y \sin \Omega}{r} \\ \sin U = \frac{r_z}{r \sin i} \end{cases}$$

and

$$\begin{cases} \cos \nu = \frac{1}{e}(\frac{a(1-e^2)}{r} - 1) \\ \sin \nu = \frac{a(1-e^2)}{eh}(\frac{\vec{r} \cdot \dot{\vec{r}}}{r}). \end{cases}$$

E. Self Consistency Test

To test if our orbit determination process is self consistent, we created an ephemeris using the orbital elements that we obtained from the Method of Gauss and compared it to the JPL Horizons ephemeris. All values and percent differences are reported in Table VI.

Element	Mean	JPL Mean	Units	Standard Deviation	Percent Difference
a	1.80092	1.87613	au	0.02177	-4.00898
e	0.37258	0.39482		0.00667	-5.63387
i	1.54390	1.60843	deg	0.01970	-4.01235
Omega	122.032	121.804	deg	0.07415	0.18757
omega	163.422	163.439	deg	0.03744	-0.00981
M	357.804	356.87	deg	0.02642	0.26180

TABLE V
COMPARISON OF ORBITAL ELEMENTS AGAINST JPL HORIZONS.

F. Results

The Method of Gauss converged on the three observations in Table V after 120 iterations. Monte Carlo simulations were also ran 10,000 times. The calculated orbital elements, Monte Carlo means and standard deviations, JPL Horizons predicted values, and percent differences are displayed in Table V.

Table VI compares the ephemeris generation results with the JPL Horizons predicted values at the time of the last observation using the middle observation as a reference.

Element	Calculated	JPL	Percent Diff.
RA	16:27:55.753	16:27:10.73	0.076
DEC	-18:45:44.27	-18:41:01.8	0.42

TABLE VI
COMPARISON OF CALCULATED EPHEMERIS VALUES AGAINST JPL HORIZONS.

IV. DISCUSSION

A. Comparison against JPL Horizons

Our calculations of RA and DEC were quite similar to the values reported on JPL Horizons. In terms of the July 3rd observation, JPL Horizons reported the RA and Dec of 2003 HA22 as 16:27:10.73 and -18:41:01.8, respectively. Our value for RA differed only by 45 seconds, while our value for DEC differed by 4 arcseconds. In regards to both RA and DEC, JPL Horizons produced slightly lower values than our calculations. For the observation at NIRo on July 8th, JPL Horizons displayed the asteroid's RA as 16:27:10.73, and the Dec as -18:41:01.8, while we had calculated 17:53:19.54 and -20:29:11.2 respectively. In this case, our values for RA differed by quite a lot. The values for RA and Dec for this observation were a bit lower than our calculations. For our final observation on July 15th, JPL Horizons reported 16:25:38.34 as the asteroid's RA and -18:40:50.0 as the asteroid's Dec. Our calculated value for RA differed by 0.13 seconds, while our value for Dec differed by 0.7 arcseconds. Again, JPL Horizons had slightly higher values than ours. Overall, our values for RA and Dec were rather consistent with the values computed on JPL Horizons; the largest errors did not exceed a few seconds or arcseconds. Thus, the information on JPL Horizons reaffirms the relative accuracy of our calculations.

B. Potential Sources of Error

Factors that affected the quality of our results may include the visual quality of our images, however, inconsistencies in our images have been minimized through the image reduction and alignment process. Additionally, the quality of our results is always subject to human error, such as misreading a number or performing an incorrect calculation. However, we believe that this is not the case. Even so, there are multiple things that could be done to improve our results. One could be to use observations that are further apart, allowing us to better measure the asteroid's trip across the sky. Another could be to use more than three observations; this would allow us to produce more accurate average calculations of RA, Dec, and magnitude. Additionally, we could implement a differential correction procedure to each set of data, which would further refine our results.

C. SWIFT Integration

In addition to our calculations, we also conducted a simulation under the guidance of researchers from the Southwest Research Institute (SwRI), in which we attempted to determine the fate of our asteroid within the next 50 Myr. As we processed our data with the Swift software, we found that in 70% of test cases our asteroid had too small a perihelion, indicating that it got too close to the Sun. Thus, our SwRI simulations conclude that 2003 HA22 is likely to perish due to too small a perihelion. Since only 2 of our 48 test particles struck the Earth, there is minimal danger posed by our asteroid to the Earth within this timeframe.

Acknowledgements

We graciously thank ONL 8 (N. Shah, E. Lu, J. Tan) for the use of their data in this report and in our OD code, and for invaluable math calculation aid. We would like to thank Dr. Cassandra Fallscheer, Dr. Michael Hannawald for leading the program, the TAs for supporting and helping us through the process, and everyone at the Summer Science Program for providing us with this opportunity. We would also like to thank Dr. Julien Salmon and Dr. Raluca Rufu for introducing us to solar system integration how to use SWIFT to simulate our asteroids.

References

[1] *Asteroids*. URL: https://solarsystem.nasa.gov/asteroids-comets-and-meteors/asteroids/overview?page=0&per_page=40&order=name+asc&search=&condition_1=101%3Aparent_id&condition_2=asteroid%3Abody_type%3Ailike (visited on 07/24/2021).

[2] *Asteroids: What Are They and Where Do They Come From?* en-US. July 2014. URL: https://skyandtelescope.org/astronomy-resources/astronomy-questions-answers/what-are-asteroids/ (visited on 07/24/2021).

[3] *Comets*. URL: https://solarsystem.nasa.gov/asteroids-comets-and-meteors/comets/overview?page=0&per_page=40&order=name+asc&search=&condition_1=102%3Aparent_id&condition_2=comet%3Abody_type%3Ailike (visited on 07/24/2021).

[4] *Horizons web-interface*. URL: https://ssd.jpl.nasa.gov/horizons.cgi (visited on 07/24/2021).

[5] Sarah Loff. *NASA's Search for Asteroids to Help Protect Earth and Understand Our History*. und. Text. Apr. 2014. URL: http://www.nasa.gov/content/nasas-search-for-asteroids-to-help-protect-earth-and-understand-our-history (visited on 07/22/2021).

[6] *Mars-crossing Asteroids — Space Reference*. URL: https://www.spacereference.org/category/mars-crossing-asteroids (visited on 07/22/2021).

[7] *Near-Earth asteroid*. en. URL: https://www.sciencedaily.com/terms/near-earth_asteroid.htm (visited on 07/22/2021).

[8] *PROMPT Description*. URL: https://users.physics.unc.edu/~reichart/prompt2.html (visited on 07/22/2021).

[9] *The Probability of Collisions with Earth*. URL: https://www2.jpl.nasa.gov/sl9/back2.html (visited on 07/22/2021).

[10] *What is the Kuiper Belt?* en. May 2020. URL: https://spacecenter.org/what-is-the-kuiper-belt/ (visited on 07/24/2021).